PAPER • OPEN ACCESS

Complete conversion between one and two photons in nonlinear waveguides: theory of dispersion engineering

New Journal of Physics
The open access journal at the forefront of physics

Deutsche Physikalische Gesellschaft DPG
IOP Institute of Physics

Published in partnership with: Deutsche Physikalische Gesellschaft and the Institute of Physics

OPEN ACCESS

RECEIVED
6 October 2021

REVISED
10 May 2022

ACCEPTED FOR PUBLICATION
25 May 2022

PUBLISHED
13 June 2022

PAPER

Complete conversion between one and two photons in nonlinear waveguides: theory of dispersion engineering

Alexander S Solntsev[1,*], Sergey V Batalov[2,3], Nathan K Langford[1] and Andrey A Sukhorukov[4]

[1] School of Mathematical and Physical Sciences, University of Technology Sydney, 15 Broadway, Ultimo NSW 2007, Australia
[2] Institute of Metal Physics, UB RAS, Sofia Kovalevskaya str., 18, Ekaterinburg 620108, Russia
[3] Institute of Physics and Technology, Ural Federal University, Mira str. 19, Ekaterinburg 620002, Russia
[4] ARC Centre of Excellence for Transformative Meta-Optical Systems (TMOS), Department of Electronic Materials Engineering, Research School of Physics, Australian National University, Canberra ACT 2601, Australia
[*] Author to whom any correspondence should be addressed.

E-mail: alexander.solntsev@uts.edu.au and andrey.sukhorukov@anu.edu.au

Keywords: waveguide, dispersion engineering, coherent photon conversion

Abstract

High-efficiency photon-pair production is a long-sought-after goal for many optical quantum technologies, and coherent photon conversion (CPC) processes are promising candidates for achieving this. We show theoretically how to control coherent conversion between a narrow-band pump photon and broadband photon pairs in nonlinear optical waveguides by tailoring frequency dispersion for broadband quantum frequency mixing. We reveal that complete deterministic conversion as well as pump-photon revival can be achieved at a finite propagation distance. We also find that high conversion efficiencies can be realised robustly over long propagation distances. These results demonstrate that dispersion engineering is a promising way to tune and optimise the CPC process.

1. Introduction

Optical nonlinearities play a vital role in the development of quantum-enhanced technologies based on quantum optics and photonic quantum information [1–4]. Typically realised in the optical regime through interactions with individual atomic systems [5–7] or atomic media [8–13], such nonlinearities are very weak at the few-photon level unless enhanced by, e.g., cavity confinement [14, 15], coherent ensemble effects [8, 9, 16] or strong classical pump fields [12, 17]. In 2001, the pioneering KLM proposal [1] demonstrated that direct photon–photon nonlinearities could be circumvented using the strong local nonlinearity provided by avalanche photodetection, with feedforward and teleportation, to enable efficient, fault-tolerant quantum computation with linear optics [2]. While subsequent proposals have greatly reduced the significant physical resource overheads of a linear optics approach [18–20], nonlinear optical quantum computing [21–24] still provides an enticing alternative, with strong, direct photon–photon nonlinearities promising to minimise the intensive resource requirements entailed by probabilistic interactions.

After initial proposals [21–23] based on photon–photon cross-phase modulation, developments in nonlinear optical quantum computing slowed for some time after several theoretical 'no-go' theorems (e.g. [25, 26]). These suggested the goal of directly realising multiphoton gates between travelling photon pulses using optical nonlinearities faced fundamental roadblocks, due to finite-bandwidth and spectral entanglement effects that create a trade-off between nonlinear interaction strengths and gate fidelities. Later, Langford *et al* introduced a new photon-level nonlinear process, coherent photon conversion (CPC), that could sidestep these issues and provide a versatile building block for a new, scaleable quantum computing architecture [24]. Generalising well-established concepts in spontaneous parametric down-conversion (SPDC) and single-photon up-conversion [10, 17, 27], CPC provides a nonlinear module that enables deterministic multiphoton gates, high-quality heralded single- and multiphoton states free from

higher-order imperfections, and robust, high-efficiency detection. Initial analysis suggested similar fundamental roadblocks also limit the performance of CPC-based operations for pulsed (broadband) photons [28]. Subsequent work, however, including by the authors of reference [28], has identified operational paradigms for CPC and other nonlinear optical quantum operations that potentially circumvent these issues [29–34], for example by using dispersion and group-velocity engineering to control the pulse interactions [29, 35, 36] or atom-mediated pulse interactions [27, 30]. Despite these promising steps, however, it remains an important open question to identify the ultimate limitations to high-efficiency CPC operations.

SPDC, the major workhorse for nonclassical light sources in quantum optics and quantum information experiments, has found important application in two different operating paradigms. When implemented with pulsed pump lasers, SPDC produces more narrowband, possibly factorable photon pairs, enabling the synchronised, multipair photon production that is vital for quantum computing [37–40], quantum networking [41–43] and quantum sensing [44, 45] applications. When implemented with narrowband pump lasers, SPDC leads to highly broadband, spectrally entangled output photons, which can be important for quantum communication, imaging and sensing tasks [46–50].

To date, experimental and theoretical investigations of CPC have mostly focused on the broadband pump paradigm. In this regime, experimental demonstrations include conversion of a single photon to two in an optical fiber [24], and two to one in a nonlinear waveguide [51]. While the demonstrated conversion efficiency was relatively low in these first experiments, it can be improved by orders of magnitude by using strongly nonlinear materials and optimizing the waveguide geometry [52], based on solutions derived in the low-conversion regime. In the narrowband-pump regime, it has also been predicted that complete conversion of a single pump photon to two down-converted photons can be achieved in a nonlinear waveguide with quadratic frequency dispersion [53, 54], provided the sufficient nonlinearity is available. Recent progress demonstrates significant advances in that respect [55], opening the opportunities for future experimental realisations of efficient single-photon splitting.

Following our original proposal [56], in this work, we show how dispersion engineering can be used to tune the photon-conversion process. This addresses a key open goal in this context, which is to study the optimal conditions for achieving deterministic photon conversion both from a single photon to a pair and also backward. We study a range of dispersion scenarios and show that we can reach 100% forward and backward conversion efficiency at a finite propagation length. We also show that it is possible to realise robust conversion between one and two photons, where high conversion efficiencies can be realised over a large propagation distance range. These are nontrivial results due to the complex dynamics involving the one- and two-photon states across a broad optical frequency spectrum.

2. Model

2.1. Conceptual framework

We start by considering the coherent conversion of a pump photon with a central frequency ω_p into signal and idler photons, see figure 1(a). This process can be realized in media with cubic nonlinearity through four-wave mixing involving a high-power control wave at a different frequency ω_c [24]. For narrow-band spectra (i.e. single frequency modes) of the input photon and the control wave, the signal (index s) and idler (index i) frequencies are related due to the energy conservation as $\omega_s + \omega_i = \omega_p + \omega_c$. On the other hand, the splitting between the two photon frequencies can be arbitrary, $\omega_s - \omega_i = \Omega$, effectively creating a multimode regime for the generated biphoton with entangled frequencies. In the following, we show how to utilize a larger number of CPC channels corresponding to different detunings Ω (figure 1(b)) in order to reach complete photon conversion in the forward and backward directions.

The dynamics of the CPC is determined by the phase mismatch of the four-wave-mixing process across a range of photon frequencies, $\Delta\beta(\Omega) = \beta(\omega_s) + \beta(\omega_i) - \beta(\omega_p) - \beta(\omega_c)$, where β is the propagation constant of the waveguide mode at the corresponding optical frequency. Whereas it is generally accepted that most efficient conversion occurs in the regime of phase matching [52], the shape of the mismatch dependence around the phase-matching point plays a critically important role in the high-conversion regime. We consider coupled equations for the single and two-photon wavefunctions in the strong conversion regime [53], and establish their mathematical equivalence to the fundamentally important phenomenon of the decay of a discrete atomic state to a continuum [57], however the role of temporal evolution is replaced by the propagation distance along the waveguide (z). Therefore, by choosing a particular waveguide length, we can access any intermediate stage of the decay dynamics.

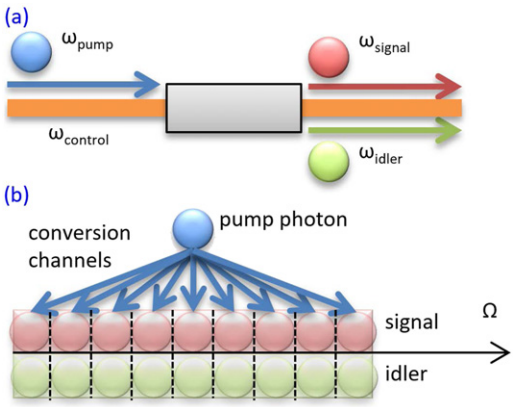

Figure 1. (a) The concept of coherent conversion of a pump photon into signal and idler photons with frequencies ω_s and ω_i, respectively. (b) Photon conversion channels associated with different frequency detunings between the signal and idler photons. Utilising a larger number of CPC channels by increasing the generated photon-pair bandwidth can drastically increase the efficiency of the process.

2.2. Theoretical model

Now let us derive a model following reference [52] and restricting four-wave mixing to only one polarization component in a single-mode waveguide. We note that in this case we will be neglecting spurious nonlinear effects (including competing four-wave-mixing processes) [58]. In this case the propagating field can be written in the form

$$\hat{E}(z,t) = \sqrt{\frac{\hbar}{4\pi\varepsilon_0 c A_{\text{eff}}}}\int_0^\infty \mathrm{d}\omega \sqrt{\frac{\omega}{n(\omega)}}\hat{a}(\omega,z)\mathrm{e}^{-\mathrm{i}\omega t} + \text{h.c.}, \tag{1}$$

where effective area of the waveguide mode A_{eff} is taken to be the same for all frequency components in the waveguide. Length L of the fiber is assumed to be large enough for the continuous limit to be valid. Note that operators $\hat{a}(\omega,z)$ in equation (1) are chosen to be dimensional with units of $(\delta\omega)^{-1/2}$ [59], where $\delta\omega$ is the frequency spacing due to periodic boundary conditions $\delta\omega = 2\pi/T$ and $T = L/c$ is the quantization time.

In absence of nonlinearity, evolution of operators $\hat{a}$ can be found [60] to be $\hat{a}(\omega,z) = \hat{a}_0\,\mathrm{e}^{\mathrm{i}\beta(\omega)z}$, where $\beta(\omega) = n(\omega)\omega/c$. In the nonlinear medium operators $\hat{a}_0$ become functions of coordinate and frequency. If the strong control wave can be taken as classical ($\hat{a}_0(\omega_c,z) \equiv A_c(z)$) and undepleted ($|A_c(z)|^2 = |A_c(0)|^2$), then the evolution of the weak single-photon pump and generated signal and idler modes is governed by the following set of equations [52] [5]

$$\frac{\partial\hat{a}_0(\omega_p,z)}{\partial z} = 2\mathrm{i}\gamma\sqrt{P_c\zeta_p}\frac{T}{2\pi}\int \mathrm{d}\omega_s\,\hat{a}_0(\omega_s,z)\hat{a}_0(\omega_c+\omega_p-\omega_s,z)\mathrm{e}^{\mathrm{i}(\Delta k-\gamma P_c)z} + 2\mathrm{i}\gamma P_c\hat{a}_0(\omega_p,z), \tag{2}$$

$$\frac{\partial\hat{a}_0(\omega_s,z)}{\partial z} = 2\mathrm{i}\gamma\sqrt{P_c\zeta_p}\hat{a}_0^\dagger(\omega_c+\omega_p-\omega_s,z)\hat{a}_0(\omega_p,z)\mathrm{e}^{-\mathrm{i}(\Delta k-\gamma P_c)z} + 2\mathrm{i}\gamma P_c\hat{a}_0(\omega_s,z). \tag{3}$$

Here $\gamma(\omega_s) = 3\chi^{(3)}\omega_s/[2\varepsilon_0 c^2 n^2(\omega_s)A_{\text{eff}}]$ is the standard waveguide parameter. We will assume that the value of γ is approximately the same for all the frequency modes [61]. Parameter $P_c = 2\pi\hbar\omega_c T^{-2}|A_c|^2$ measures the peak power of the strong control wave. Parameter $\zeta_p = 2\pi\hbar\omega_p T^{-2}$ is defined so that $P_p = \zeta_p \times \langle a^\dagger(\omega_p,0)a(\omega_p,0)\rangle$ is the photon population of the weak pump at the entrance of the medium. In case of a single-photon pump we have $P_p = \zeta_p \times T/(2\pi)$. Δk is a phase mismatch based on the waveguide geometry. The total phase mismatch $\Delta\beta = -(\Delta k + \gamma P_c)$ can be modified dynamically by changing the strong pump power.

Now let us introduce the function for the pump photon dynamics

$$U(z) = \mathrm{e}^{2\mathrm{i}\,\gamma P_c z}\frac{2\pi}{T}\langle 0|\hat{a}_0(\omega_p,0)\hat{a}_0^\dagger(\omega_p,z)|0\rangle. \tag{4}$$

This is the probability amplitude to find a weak pump photon at distance z (creation operator at distance z) provided that there was one photon at distance $z = 0$ (annihilation operator at the origin $z = 0$). Factor

[5] Equation (17) in [52] contains a typo. Factor $2\pi/T$ should be replaced by $T/2\pi$.

$2\pi/T$ accounts for units of operators $\hat{a}_0$ and exponential factor is introduced for convenience. Taking coordinate derivative and comparing with equation (2) we obtain the following equation [53]

$$\frac{\mathrm{d}U}{\mathrm{d}z} = -\mathrm{i}\chi\frac{T}{2\pi}\int \mathrm{d}\omega_s\, V(\omega_s, z), \tag{5}$$

where $\chi = 2\gamma\sqrt{P_c P_p}$. New quantity $V(\omega, z)$ in equation (5) is defined as follows

$$V(\omega_s, z) = \left(\frac{2\pi}{T}\right)^{3/2} \mathrm{e}^{\mathrm{i}(3\gamma P_c - \Delta k)z} \times \langle 0|\hat{a}_0(\omega_p, 0)\hat{a}_0^{\dagger}(\omega_c + \omega_p - \omega_s, z)\hat{a}_0^{\dagger}(\omega_s, z)|0\rangle. \tag{6}$$

Its physical meaning is the probability amplitude to find a pair of photons ω_s and $\omega_i = \omega_c + \omega_p - \omega_s$ at distance z, provided that there was a single pump photon with frequency ω_p at distance $z = 0$. Differentiating $V(\omega_s, z)$ with respect to z we get a second equation

$$\frac{\mathrm{d}V}{\mathrm{d}z} = -\mathrm{i}\Delta\beta V - \mathrm{i}\chi U, \tag{7}$$

where we took into account that $\hat{a}_0(\omega, z)|0\rangle \equiv 0$ and $\hat{a}_0(\omega, z)\hat{a}_0^{\dagger}(\omega, z)|0\rangle \equiv T/(2\pi)|0\rangle$. Equations (5) and (7) together with 'initial conditions' $U(0) = 1$, $V(\omega, 0) = 0$ can be used to describe dynamics of our system, effectively representing solutions of the operator equations (2) and (3). The temporal dynamics for the photon pair packet can then be calculated via Fourier transform $\tilde{V}(\tau, z) = (2\pi)^{-1/2}\int_{-\infty}^{\infty} U(\omega, z)\mathrm{e}^{\mathrm{i}\omega\tau}\,\mathrm{d}\omega$. We note that in the framework of equations (5) and (7), the combined population of pump photons I_p and signal-idler pairs I_s is conserved,

$$\frac{\mathrm{d}}{\mathrm{d}z}\left[I_p(z) + I_s(z)\right] = 0, \tag{8}$$

where

$$I_p(z) = |U(z)|^2, \quad I_s(z) = \int \mathrm{d}\omega_s |V(\omega_s, z)|^2 = \int \mathrm{d}\tau |\tilde{V}(\tau, z)|^2. \tag{9}$$

With no loss of generality, in the numerical examples below we consider a normalization of variables such that $\chi T/(2\pi) = 1$. We also introduce a notation $\Omega = \omega_s - \omega_{s0}$, where ω_{s0} is a characteristic signal photon frequency.

3. Results

3.1. Complete conversion of one photon into two

Now we analyze the effects of frequency dispersion $\Delta\beta(\Omega)$ on the photon dynamics. A linear dispersion corresponds to Markovian decay and allows 100% conversion efficiency only in the limit of infinite propagation distance $z \to \infty$. In contrast, the higher-order dispersion enables complete conversion. Specifically, 100% conversion efficiency (figure 2(a)) at a finite propagation distance in normalized units $z_c = 0.83$ can be enabled by the shifted quadratic dispersion $\Delta\beta = \Omega^2 - 2.88$ (figure 2(b)). We find that there appear multiple parameter regions corresponding to the full conversion, see appendix A, whereas only specific cases we identified in previous studies [53, 54]. We note that the mathematical model of complete conversion under quadratic dispersion is equivalent to a decay of atomic state to a continuum near a photonic band-edge [62], and accordingly the effect of complete transitional decay can also happen for atoms, see appendix A for details. Interestingly, after the rebound from complete conversion, in the temporal domain an entangled state with an approximate form $|0\rangle_s|0\rangle_i + |\tau_0\rangle_s|-\tau_0\rangle_i + |-\tau_0\rangle_s|\tau_0\rangle_i$ is generated, where τ defines delay or advance for the signal/idler photons in a moving frame. Specifically, the signal and idler photons are either travelling together in the central peak or with a time delay $\pm\tau_0$ linearly growing with propagation distance z (figure 2(c)). A similar state with three peaks is also formed in the spectral domain, although the distance between the peaks remains constant with increasing z (figure 2(d)). The considered quadratic dispersion typically occurs near the degeneracy point when $\omega_s \approx \omega_i$ [58], which can be readily accessed experimentally.

3.2. Photon conversion reversal

A regime which is of particular interest in the context of photonic quantum computing is where coherent conversion can be realised in both forwards and backwards directions, allowing a pair of photons to also completely convert back into one photon, similar to Rabi oscillations [24, 52]. However, when dispersion is present, this regime is no longer possible in homogeneous waveguides. This is because the spectral distribution of the generated pair of photons interacts in a complex way with the nontrivial waveguide dispersion, and does not produce full coherent recombination in the backwards process [53, 54].

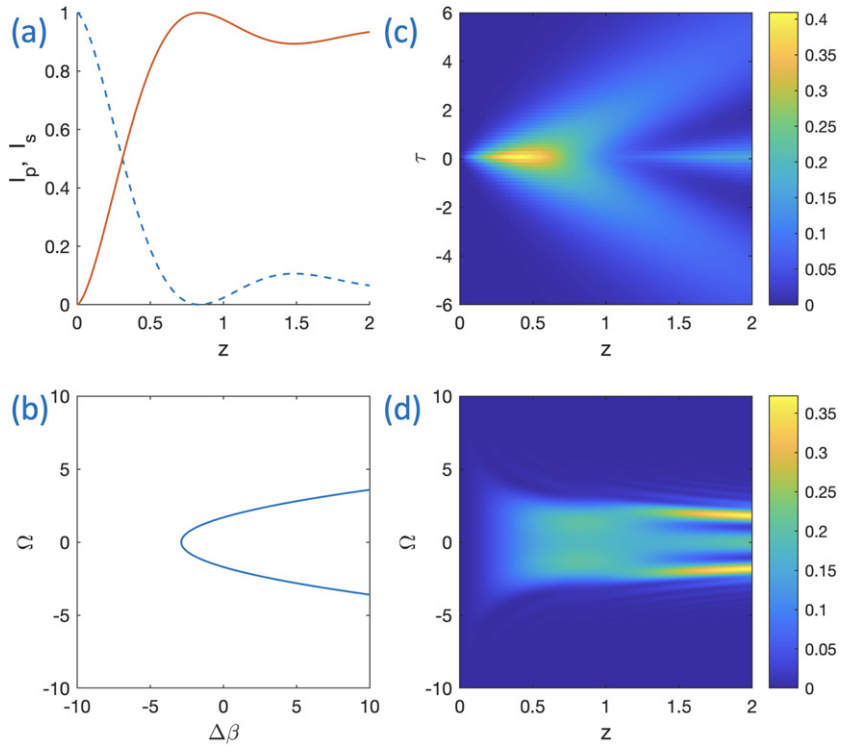

Figure 2. Complete conversion of one photon into two at a finite propagation distance ($z_c = 0.83$). (a) Pump (dashed blue) and signal/idler (solid red) photon populations vs the propagation distance z in the case of quadratic waveguide dispersion $\Delta\beta = \Omega^2 - 2.88$ shown in (b). (c) Temporal and (d) spectral dynamics of the biphoton population $|V|^2$ vs the propagation distance z.

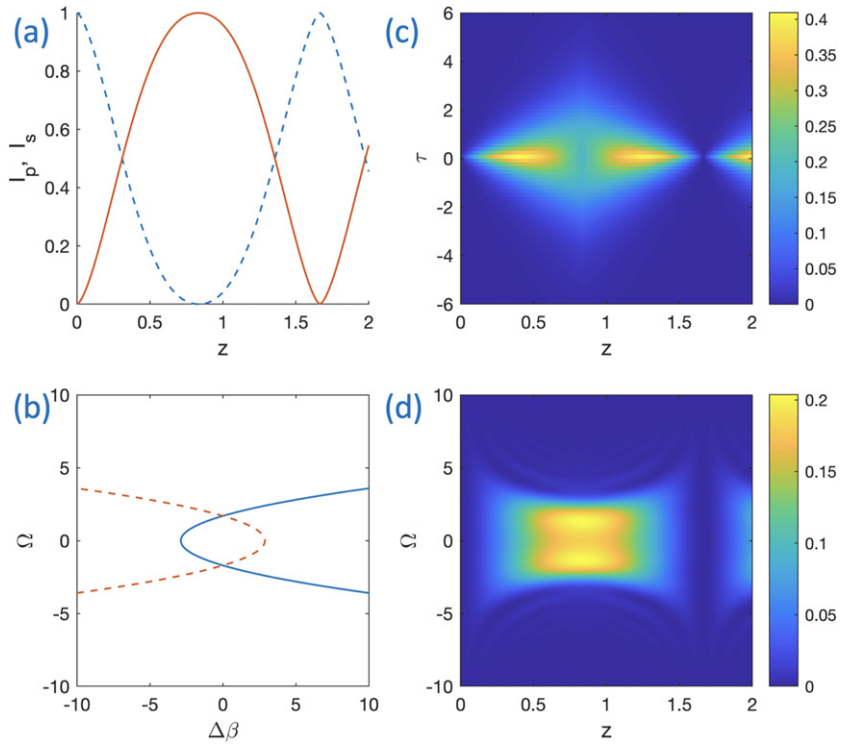

Figure 3. Forward and backward conversion between one- and two-photon states achieved by reversing the sign of the dispersion. (a) Pump (dashed blue) and signal/idler (solid red) photon populations vs the propagation distance z. (b) Quadratic waveguide dispersion $\Delta\beta = \Omega^2 - 2.88$ for $z \leqslant z_{\text{inv}} \simeq 2.53$ (solid blue line) and the specially inverted dispersion $\Delta\beta = -\Omega^2 + 2.88$ for $z > z_{\text{inv}}$ (dashed red). (c) Temporal and (d) spectral dynamics of the biphoton population $|V|^2$ vs the propagation distance z.

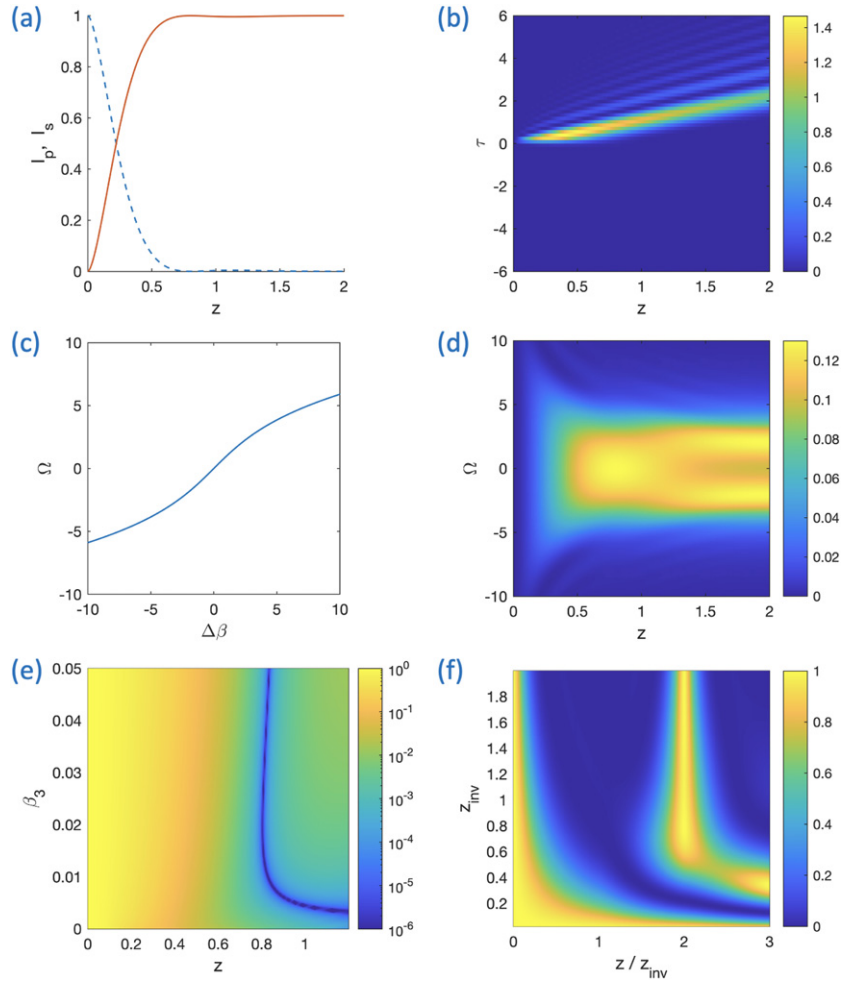

Figure 4. Robust conversion between one and two photons achieved through engineering higher-order frequency dispersion. (a) Pump (dashed blue) and signal/idler (solid red) photon populations vs the propagation distance z in the case of cubic waveguide dispersion. (b) Temporal dynamics of the biphoton population $|V|^2$ vs the propagation distance z. (c) Dispersion $\Delta\beta = \beta_3\Omega^3 + \Omega$, with $\beta_3 = 0.02$. (d) Spectral dynamics of the biphoton population $|V|^2$ vs the propagation distance z. (e) Pump photon population $|U|^2$ shown in logarithmic scale vs the propagation distance z and third-order dispersion coefficient β_3. (f) Pump photon population $|U|^2$ vs the coordinate of dispersion sign inversion z_{inv} and the normalized distance z/z_{inv} for $\beta_3 = 0.02$.

Here, however, we show that complete forward and backward conversion between one- and two-photon states can be achieved through waveguide dispersion engineering. Specifically, by inverting the sign of the dispersion $\Delta\beta \to -\Delta\beta$ at the point of maximum conversion, the photon population dynamics reverses according to the symmetry of the governing equations. Thereby, at twice the complete forward conversion distance, a biphoton converts back into a single pump photon (figure 3(a)). In this case, mirroring the dispersion at $z_{\text{inv}} \simeq 2.53$ (figure 3(b)) is sufficient, which can be achieved through a tailored waveguide engineering. The biphoton wavepacket in the temporal domain (figure 3(c)) as well as its spectrum (figure 3(d)) also show complete reversal. During this process, the phase of the original photon is shifted by π, in a similar way to the nonlinear optical control-phase gates realised in [24]. Given the complex spectral dynamics that takes place during CPC in the presence of nontrivial waveguide dispersion, it is already interesting to observe that complete reversal is still possible, and surprising that it can be achieved with such a mathematically simple dispersion modification.

3.3. Robust photon conversion mediated by higher-order dispersion

We then find that more robust operation of photon conversion can be achieved by further tailoring the higher-order waveguide dispersion. As discussed above, in the case of quadratic dispersion, the pump photon population quickly rebounds after complete conversion, which would require highly precise optimisation of the frequency dispersion and optical nonlinearity in experiments. We find that conversion with strongly reduced sensitivity to experimental inaccuracies can be achieved in waveguides with engineered cubic frequency dispersion. We show an example of 100% conversion efficiency at $z_c \simeq 0.8$ in figure 4(a), followed by an extended region of over 99.5% conversion. This flat behaviour with respect to an

increase of the propagation distance z indicates high robustness against the experimental deviations. In terms of temporal dynamics, the biphoton shows very limited spreading with a moderate, extended tail (figure 4(b)), when a tailored cubic dispersion with $\Delta\beta = \beta_3\Omega^3 + \Omega$ with $\beta_3 = 0.02$ is utilized (figure 4(c)). In the spectral domain, there are two merged peaks (figure 4(d)). We show the effect of the third-order dispersion strength on the pump photon evolution in figure 4(e). We observe that for $\beta_3 \simeq 0.02$, the zero position z_c effectively does not depend on variations of β_3, indicating robustness with respect to β_3 variations. Importantly, the robustness of back-conversion from two photons to one photon based on a general approach formulated above, where the dispersion sign is inverted at $z_{\rm inv}$, can be also enhanced by third-order dispersion optimization. We show in figure 4(f) that for a large range of $z_{\rm inv} \geqslant z_c \simeq 0.8$, there is nearly complete back-conversion with $|U|^2 \to 1$ at $z = 2z_{\rm inv}$.

4. Conclusions

In conclusion, we have shown that complete deterministic conversion between one and two photons can be achieved in nonlinear waveguides with specially engineered frequency dispersion. In particular, quadratic dispersion can facilitate 100% conversion efficiency between one and two photons in the forward and backward directions at finite propagation lengths, allowing the pump photon to complete a full oscillation. Furthermore, specially optimized cubic dispersion enables highly robust photon conversion, with strongly reduced sensitivity to potential experimental inaccuracies. This work shows that dispersion can be designed for the high-efficiency production of spectrally entangled, broadband photon pairs, with no higher-order multiphoton terms, which may provide significant benefits for use in advanced quantum communication technologies.

Acknowledgments

The authors acknowledge the support by the Australian Research Council (DE180100070, DP160100619, DP190100277). NKL is funded by the Australian Research Council Future Fellowship (FT170100399). Batalov S V acknowledges support by the Ministry of Education and Science of the Russian Federation (the theme 'Quantum', No. AAAA-A18-118020190095-4).

Data availability statement

The data that support the findings of this study are available upon reasonable request from the authors.

Appendix A. Asymptotic analysis of photon populations

Let us explore the quadratic dispersion approximation to the total phase mismatch $\Delta\beta = \Delta\beta_0 + \beta_2\Omega^2$ in more detail. Applying Laplace transform $f(s) = \int_0^\infty f(z)\mathrm{e}^{-sz}\,\mathrm{d}z$ to equations (5) and (7) and taking into account conditions at the left waveguide boundary $U(0) = 1$, $V(\Omega, 0) = 0$ we find

$$U(s) = \left[s + \frac{\alpha\sqrt{\mathrm{i}}}{\sqrt{s - \mathrm{i}\Delta\beta_0}}\right]^{-1}, \tag{A.1}$$

where $\alpha = \pi\chi^2/\sqrt{\beta_2}$. The inverse Laplace transform then yields

$$U(z) = \mathrm{e}^{\mathrm{i}\Delta\beta_0 z}\sum_k \frac{\mathrm{e}^{p_k^2 z}}{3 + \mathrm{i}\Delta\beta_0/p_k^2}\left(1 + \mathrm{erf}(p_k\sqrt{z})\right), \tag{A.2}$$

where $\mathrm{erf}(x)$ is the error function and p_k are the three roots of the following cubic equation:

$$p^3 + \mathrm{i}\Delta\beta_0 p + \alpha\sqrt{\mathrm{i}} = 0.$$

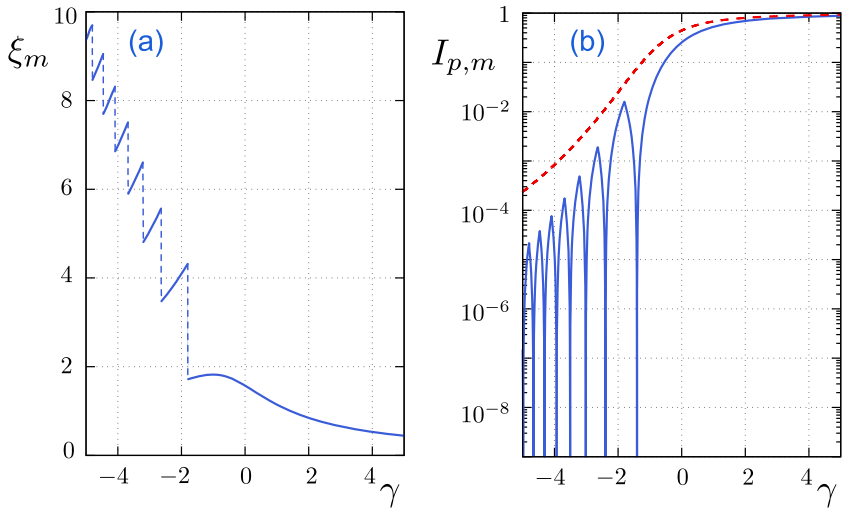

Figure A1. (a) Scaled optimal waveguide length $\xi_m(\gamma)$ corresponding to the global minimum of pump photon population. Dashed lines mark discontinuities due to changes of local minima. (b) Pump photon population at optimal waveguide lengths $I_{p,m}(\gamma) = |U(\xi_m(\gamma), \gamma)|^2$. Red dashed line in (b) corresponds to pump photon population at infinite distance according to equation (A.8).

Table A1. First five roots of $I_{p,m}(\gamma)$ and corresponding scaled waveguide lengths ξ_m.

γ	−1.4057	−2.3981	−3.0159	−3.5085	−3.9330
ξ_m	1.7895	3.6828	5.0337	6.1353	7.0843

Roots p_k can be expressed using Vieta's formula as

$$\begin{aligned} p_k &= \alpha^{1/3}\sigma_k(\gamma), \\ \sigma_k(\gamma) &= \mathrm{e}^{-\frac{\mathrm{i}\pi}{4}}\left(\zeta^k A + \zeta^{2k} B\right), \\ A &= \sqrt[3]{\frac{1}{2} + \frac{1}{2}\sqrt{1 - \frac{4\gamma^3}{27}}}, \\ B &= \frac{\gamma}{3A}, \\ k &= 0, 1, 2, \end{aligned} \tag{A.3}$$

where $\gamma = \Delta\beta_0/\alpha^{2/3}$ and $\zeta = \mathrm{e}^{2\pi\mathrm{i}/3}$ is one of the cubic roots of unity. It is convenient to introduce new spatial variable $\xi = \alpha^{2/3}z$, then solution in equation (A.2) depends on single parameter γ:

$$U(\xi, \gamma) = \mathrm{e}^{\mathrm{i}\gamma\xi}\sum_k \frac{\mathrm{e}^{\sigma_k^2\xi}}{3 + \mathrm{i}\gamma/\sigma_k^2}\left(1 + \mathrm{erf}(\sigma_k\sqrt{\xi})\right), \tag{A.4}$$

where σ_k are given by equation (A.3) and are functions of γ only.

Let us calculate the asymptotic value of the pump wave population at infinite distance. The asymptotics of error function at $z \to \infty$ is given by [63]:

$$\mathrm{erf}z \sim \begin{cases} 1 - \mathrm{e}^{-z^2}/(z\sqrt{\pi}), & z \in \Omega_1, \\ -1 - \mathrm{e}^{-z^2}/(z\sqrt{\pi}), & z \in \Omega_2, \\ -\mathrm{e}^{-z^2}/(z\sqrt{\pi}), & z \in \Omega_3, \end{cases}$$

where Ω_1, Ω_2 and Ω_3 are sectors of complex plane with $-\pi/4 < \arg z < \pi/4$, $3\pi/4 < \arg z < 5\pi/4$ and $\pi/4 < \arg z < 3\pi/4 \cup 5\pi/4 < \arg z < 7\pi/4$ respectively. As γ changes from $-\infty$ to $\gamma^* = 3/4^{1/3}$, roots $\sigma_k(\gamma)$ move in complex plane so that $\sigma_1(\gamma) \in \Omega_3$ and $\sigma_2(\gamma) \in \Omega_2$. For $\xi \to +\infty$ the contributions from

these two roots vanish:

$$e^{\sigma_1^2\xi}\left(1+\operatorname{erf}\sigma_1\sqrt{\xi}\right)\sim e^{\sigma_1^2\xi}-\frac{1}{\sigma_1\sqrt{\pi\xi}}\to 0, \tag{A.5}$$

$$e^{\sigma_2^2\xi}\left(1+\operatorname{erf}\sigma_2\sqrt{\xi}\right)\sim -\frac{1}{\sigma_2\sqrt{\pi\xi}}\to 0. \tag{A.6}$$

In equation (A.5) we used the fact that $\Re\left(z^2\right)<0$ in Ω_3 and the corresponding exponent rapidly decreases. The only term surviving at large distances comes from σ_0, which lies on the line $\arg\ z=-\pi/4$ for all γ. One can show by direct evaluation that $\lim_{x\to\infty}\operatorname{erf}\left(x\,e^{-i\pi/4}\right)=1$ and thus

$$e^{\sigma_0^2\xi}\left(1+\operatorname{erf}\sigma_0\sqrt{\xi}\right)\sim 2\,e^{\sigma_0^2\xi}, \tag{A.7}$$

where σ_0^2 is purely imaginary and the exponent is oscillatory. For $\gamma>\gamma^*$ both σ_1 and σ_2 lie on the line $\arg z=3\pi/4$ and by direct evaluation one can show that $\lim_{x\to\infty}\operatorname{erf}\left(x\,e^{i3\pi/4}\right)=-1$. Similarly to equation (A.6), these roots do not contribute to the asymptotic value and the only important term on big distances is equation (A.7). This results in the following asymptotic pump photon population (red dashed line in figure A1(b))

$$\lim_{\xi\to\infty}|U(\xi,\gamma)|^2=\frac{4}{\left(3+i\gamma/\sigma_0^2\right)^2}. \tag{A.8}$$

A mathematically equivalent problem of spontaneous emission of an atom with a resonant transition within photonic band gap was studied in [62]. Specifically, Laplace image equation (A.1) is equivalent to equation (2.18) from [62], up to a substitution $\Delta\beta_0\leftrightarrow\delta$, $\alpha\leftrightarrow -i\beta^{3/2}$. Since this problem is formulated in time domain, only asymptotic atomic population, equivalent to equation (A.8), can be observed experimentally. On the contrary, in our problem it is possible to adjust the waveguide length to achieve maximum conversion efficiency. Minimizing numerically $|U(\xi,\gamma)|^2$ with respect to ξ for different values of γ we find optimal scaled waveguide length ξ_m and therefore $z_m=\alpha^{-2/3}\xi_m$ (see figure A1(a)). It is clear from figure A1(b) that for certain values of γ the minimum pump wave population $I_{p,m}(\gamma)=|U(\xi_m(\gamma),\gamma)|^2$ becomes zero. First few such roots are shown in table A1. Discontinuities in $\xi_m(\gamma)$ observed in figure A1(a) and cusps in figure A1(b) correspond to switching between different local minima.

ORCID iDs

Alexander S Solntsev https://orcid.org/0000-0003-4981-9730
Nathan K Langford https://orcid.org/0000-0003-4338-3059
Andrey A Sukhorukov https://orcid.org/0000-0002-5116-5425

References

[1] Knill E, Laflamme R and Milburn G J 2001 A scheme for efficient quantum computation with linear optics *Nature* **409** 46–52
[2] Kok P, Munro W J, Nemoto K, Ralph T C, Dowling J P and Milburn G J 2007 Linear optical quantum computing with photonic qubits *Rev. Mod. Phys.* **79** 135–74
[3] Schnabel R, Mavalvala N, McClelland D E and Lam P K 2010 Quantum metrology for gravitational wave astronomy *Nat. Commun.* **1** 121
[4] Bartlett S D, Sanders B C, Braunstein S L and Nemoto K 2002 Efficient classical simulation of continuous variable quantum information processes *Phys. Rev. Lett.* **88** 097904
[5] Turchette Q A, Hood C J, Lange W, Mabuchi H and Kimble H J 1995 Measurement of conditional phase-shifts for quantum logic *Phys. Rev. Lett.* **75** 4710–3
[6] Volz J, Scheucher M, Junge C and Rauschenbeutel A 2014 Nonlinear π phase shift for single fibre-guided photons interacting with a single resonator-enhanced atom *Nat. Photon.* **8** 965–70
[7] Semiao F L and Vidiella-Barranco A 2005 Effective cross-Kerr nonlinearity and robust phase gates with trapped ions *Phys. Rev.* A **72** 064305
[8] Beck K M, Hosseini M, Duan Y and Vuletić V 2016 Large conditional single-photon cross-phase modulation *Proc. Natl Acad. Sci. USA* **113** 9740–4
[9] Tiarks D, Schmidt S, Rempe G and Durr S 2016 Optical π phase shift created with a single-photon pulse *Sci. Adv.* **2** e1600036
[10] Ou Z Y and Mandel L 1988 Violation of Bell's inequality and classical probability in a two-photon correlation experiment *Phys. Rev. Lett.* **61** 50–3
[11] Fiorentino M, Voss P L, Sharping J E and Kumar P 2002 All-fiber photon-pair source for quantum communications *IEEE Photonics Technol. Lett.* **14** 983
[12] Reim K F, Nunn J, Lorenz V O, Sussman B J, Lee K C, Langford N K, Jaksch D and Walmsley I A 2010 Towards high-speed optical quantum memories *Nat. Photon.* **4** 218–21
[13] Fabre C, Pinard M, Bourzeix S, Heidmann A, Giacobino E and Reynaud S 1994 Quantum-noise reduction using a cavity with a movable mirror *Phys. Rev.* A **49** 1337–43

[14] Hood C J, Chapman M S, Lynn T W and Kimble H J 1998 Real-time cavity QED with single atoms *Phys. Rev. Lett.* **80** 4157–60
[15] Gröblacher S, Hammerer K, Vanner M R and Aspelmeyer M 2009 Observation of strong coupling between a micromechanical resonator and an optical cavity field *Nature* **460** 724–7
[16] Julsgaard B, Sherson J, Cirac J I, Fiurášek J and Polzik E S 2004 Experimental demonstration of quantum memory for light *Nature* **432** 482–6
[17] Vandevender A P and Kwiat P G 2004 High efficiency single photon detection via frequency up-conversion *J. Mod. Opt.* **51** 1433–45
[18] Nielsen M A 2004 Optical quantum computation using cluster states *Phys. Rev. Lett.* **93** 040503
[19] Browne D E and Rudolph T 2005 Resource-efficient linear optical quantum computation *Phys. Rev. Lett.* **95** 010501
[20] Nickerson N and Bombin H 2018 Measurement based fault tolerance beyond foliation (arXiv:1810.09621)
[21] Munro W J, Nemoto K, Beausoleil R G and Spiller T P 2005 High-efficiency quantum-nondemolition single-photon-number-resolving detector *Phys. Rev.* A **71** 033819
[22] Nemoto K and Munro W J 2004 Nearly deterministic linear optical controlled-not gate *Phys. Rev. Lett.* **93** 250502
[23] Franson J D, Jacobs B C and Pittman T B 2004 Quantum computing using single photons and the Zeno effect *Phys. Rev.* A **70** 062302
[24] Langford N K, Ramelow S, Prevedel R, Munro W J, Milburn G J and Zeilinger A 2011 Efficient quantum computing using coherent photon conversion *Nature* **478** 360–3
[25] Shapiro J H 2006 Single-photon Kerr nonlinearities do not help quantum computation *Phys. Rev.* A **73** 062305
[26] Gea-Banacloche J 2010 Impossibility of large phase shifts via the giant Kerr effect with single-photon wave packets *Phys. Rev.* A **81** 043823
[27] Koshino K 2009 Down-conversion of a single photon with unit efficiency *Phys. Rev.* A **79** 013804
[28] Viswanathan B and Gea-Banacloche J 2015 Multimode analysis of a conditional phase gate based on second-order nonlinearity *Phys. Rev.* A **92** 042330
[29] Xia K Y, Johnsson M, Knight P L and Twamley J 2016 Cavity-free scheme for nondestructive detection of a single optical photon *Phys. Rev. Lett.* **116** 023601
[30] Brod D J and Combes J 2016 Passive CPHASE gate via cross-Kerr nonlinearities *Phys. Rev. Lett.* **117** 080502
[31] Viswanathan B and Gea-Banacloche J 2018 Analytical results for a conditional phase shift between single-photon pulses in a nonlocal nonlinear medium *Phys. Rev.* A **97** 032314
[32] Chudzicki C, Chuang I L and Shapiro J H 2013 Deterministic and cascadable conditional phase gate for photonic qubits *Phys. Rev.* A **87** 042325
[33] Niu M Y, Chuang I L and Shapiro J H 2018 Qudit-basis universal quantum computation using $\chi^{(2)}$ interactions *Phys. Rev. Lett.* **120** 160502
[34] Lamont M R, Kuhlmey B T and de Sterke C M 2008 Multi-order dispersion engineering for optimal four-wave mixing *Opt. Express* **16** 7551–63
[35] Mosley P J, Lundeen J S, Smith B J, Wasylczyk P, U'Ren A B, Silberhorn C and Walmsley I A 2008 Heralded generation of ultrafast single photons in pure quantum states *Phys. Rev. Lett.* **100** 133601
[36] Halder M, Fulconis J, Cemlyn B, Clark A, Xiong C, Wadsworth W J and Rarity J G 2009 Nonclassical two-photon interference with separate intrinsically narrowband fibre sources *Opt. Express* **17** 4670–6
[37] Lanyon B P, Weinhold T J, Langford N K, Barbieri M, James D F V, Gilchrist A and White A G 2007 Experimental demonstration of a compiled version of Shor's algorithm with quantum entanglement *Phys. Rev. Lett.* **99** 250505
[38] Walther P, Resch K J, Rudolph T, Schenck E, Weinfurter H, Vedral V, Aspelmeyer M and Zeilinger A 2005 Experimental one-way quantum computing *Nature* **434** 169–76
[39] Solntsev A S and Sukhorukov A A 2017 Path-entangled photon sources on nonlinear chips *Rev. Phys.* **2** 19–31
[40] Zhong H-S *et al* 2018 12-photon entanglement and scalable scattershot boson sampling with optimal entangled-photon pairs from parametric down-conversion *Phys. Rev. Lett.* **121** 250505
[41] Duan L-M, Lukin M D, Cirac J I and Zoller P 2001 Long-distance quantum communication with atomic ensembles and linear optics *Nature* **414** 413–8
[42] Barrett S D and Kok P 2005 Efficient high-fidelity quantum computation using matter qubits and linear optics *Phys. Rev.* A **71** 060310
[43] Nunn J, Langford N K, Kolthammer W S, Champion T F M, Sprague M R, Michelberger P S, Jin X-M, England D G and Walmsley I A 2013 Enhancing multiphoton rates with quantum memories *Phys. Rev. Lett.* **110** 133601
[44] Thomas-Peter N *et al* 2011 Integrated photonic sensing *New J. Phys.* **13** 055024
[45] Xiang G Y, Higgins B L, Berry D W, Wiseman H M and Pryde G J 2011 Entanglement-enhanced measurement of a completely unknown optical phase *Nat. Photon.* **5** 43–7
[46] Humphreys P C, Kolthammer W S, Nunn J, Barbieri M, Datta A and Walmsley I A 2014 Continuous-variable quantum computing in optical time-frequency modes using quantum memories *Phys. Rev. Lett.* **113** 130502
[47] Brecht B, Reddy D V, Silberhorn C and Raymer M G 2015 Photon temporal modes: a complete framework for quantum information science *Phys. Rev.* X **5** 041017
[48] Barreiro J T, Langford N K, Peters N A and Kwiat P G 2005 Generation of hyperentangled photon pairs *Phys. Rev. Lett.* **95** 260501
[49] Erkmen B I and Shapiro J H 2010 Ghost imaging: from quantum to classical to computational *Adv. Opt. Photon.* **2** 405–50
[50] Solntsev A S, Kumar P, Pertsch T, Sukhorukov A A and Setzpfandt F 2018 $LiNbO_3$ waveguides for integrated SPDC spectroscopy *APL Photonics* **3** 021301
[51] Guerreiro T *et al* 2014 Nonlinear interaction between single photons *Phys. Rev. Lett.* **113** 173601
[52] Dot A, Meyer-Scott E, Ahmad R, Rochette M and Jennewein T 2014 Converting one photon into two via four-wave mixing in optical fibers *Phys. Rev.* A **90** 043808
[53] Antonosyan D A, Solntsev A S and Sukhorukov A A 2014 Single-photon spontaneous parametric down-conversion in quadratic nonlinear waveguide arrays *Opt. Commun.* **327** 22–6
[54] Yanagimoto R, Ng E, Jankowski M P, Onodera T, Fejer M M and Mabuchi. H 2020 Broadband parametric downconversion as a discrete-continuum Fano interaction (arXiv:2009.01457)
[55] Flórez J, Lundeen J S and Chekhova M V 2020 Pump depletion in parametric down-conversion with low pump energies *Opt. Lett.* **45** 4264–7
[56] Solntsev A S and Sukhorukov A A 2015 Complete conversion of one to two photons in dispersion-engineered nonlinear waveguides *CLEO: QELS—Fundamental Science, CLEO_QELS*

[57] Akulin V M 2014 *Dynamics of Complex Quantum Systems* 2nd edn (New York: Springer)
[58] Solntsev A S, Sukhorukov A A, Neshev D N and Kivshar Y S 2012 Photon-pair generation in arrays of cubic nonlinear waveguides *Opt. Express* **20** 27441–6
[59] Blow K J, Loudon R, Phoenix S J D and Shepherd T J 1990 Continuum fields in quantum optics *Phys. Rev.* A **42** 4102–14
[60] Huttner B, Serulnik S and Ben-Aryeh Y 1990 Quantum analysis of light propagation in a parametric amplifier *Phys. Rev.* A **42** 5594–600
[61] Agrawal G P 2013 *Nonlinear Fiber Optics* 5th edn (New York: Academic)
[62] John S and Quang T 1994 Spontaneous emission near the edge of a photonic band gap *Phys. Rev.* A **50** 1764–9
[63] Olde Daalhuis A B, Chapman S J, King J R, Ockendon J R and Tew R H 1995 Stokes phenomenon and matched asymptotic expansions *SIAM J. Appl. Math.* **55** 1469–83